

A high visibility Hong-Ou-Mandel interference via a time-resolved coincidence measurement

Yoshiaki Tsujimoto,¹ Yukihiro Sugiura,¹ Motoki Tanaka,¹ Rikizo Ikuta,¹ Shigehito Miki,² Taro Yamashita,² Hiroataka Terai,² Mikio Fujiwara,³ Takashi Yamamoto,¹ Masato Koashi,⁴ Masahide Sasaki,³ and Nobuyuki Imoto¹

¹*Graduate School of Engineering Science, Osaka University, Toyonaka, Osaka 560-8531, Japan*

²*Advanced ICT Research Institute, National Institute of Information and Communications Technology (NICT), Kobe 651-2492, Japan*

³*Advanced ICT Research Institute, National Institute of Information and Communications Technology (NICT), Koganei, Tokyo 184-8795, Japan*

⁴*Photon Science Center, The University of Tokyo, Bunkyo-ku, 113-8656, Japan*

We report on the observation of a high visibility Hong-Ou-Mandel interference of two heralded photons emitted from a spontaneous parametric down conversion (SPDC) pumped by continuous-wave (cw) light. A non-degenerate photon pair at 1541 nm and 1580 nm is generated by cw-pumped SPDC through a periodically poled lithium niobate waveguide. The heralded single photon at 1541 nm is prepared by the detection of the photon at 1580 nm. We performed the experiment of the Hong-Ou-Mandel interference between heralded single photons in separated time bins and observed a high visibility interference. All detectors we used are superconducting nanowire single-photon detectors and an overall temporal resolution of the photon detection is estimated as 85 ps, which is sufficiently shorter than the coherence time of the heralded photons.

PACS numbers: 03.67.Hk, 42.50.-p, 42.50.Ex

I. INTRODUCTION

Generation, manipulation and measurement of photonic quantum states are prerequisites for many applications of quantum information processing. A high visibility Hong-Ou-Mandel (HOM) interference [1] of photons generated by independent photon sources is an important issue for fulfilling such requirements [2–5]. So far, many of such experiments have been performed with photons generated from spontaneous parametric down conversion (SPDC) pumped by ultrafast pulsed lasers [6–12]. In such experiments, the timing synchronization of the photons from the separated sources is achieved by the spectral filtering of the photons such that their coherence time is longer than that of the pump light and the adjustment of the optical path lengths for a high visibility interference. On the other hand, if timing resolutions of the photon detectors is sufficiently shorter than the coherence time of the photons, the temporal indistinguishability of the photons can be guaranteed by the coincidence detection with such a high timing resolution [13]. In this case, even when the photons are generated by a cw pump laser, post analysis of the timings of the photon detections allows us to select photons having a sufficient temporal overlap. One of the advantages of this method is that there is no need to perform the active synchronizations of the photon sources. Such an experiment has been demonstrated in Ref. [14–17]. In Ref. [14], they performed the experiment of the HOM interference between two photons independently prepared by SPDC with a cw pump light, and observed a visibility of 0.77. However, in order to perform various kinds of applications, such as quantum repeaters [18, 19], quantum relays [20, 21], measurement-device-independent quantum key distribution (QKD) [22–24], and distributed quan-

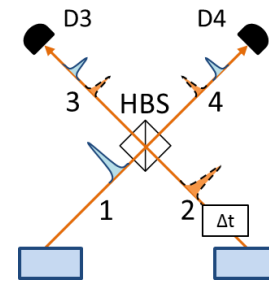


FIG. 1. (Color online) The schematic diagram of the HOM interference using independent photon sources. The relative delay is adjusted by changing the optical path length in mode 2 in the case of the pulse pumped heralded single photons. In the case of the cw pumped heralded single photons, the relative delay is adjusted by changing the detection timings of the heralding photons.

tum computation [25], a higher visibility will be desirable. In this paper, we report on a demonstration of such a high-visibility HOM interference between two photons in the cw-pumped regime with high-resolution photon detectors. In the experiment, we introduced an extended method to observe an intrinsic value of the interference visibility. We observed a visibility of 0.87 ± 0.04 , which clearly exceeds the previous result [14]. In addition, we derived a simple relationship between the visibility of the HOM interference and the second order intensity correlation function of the input light and background photons, and confirmed that the experimental results are in a good agreement with the relationship.

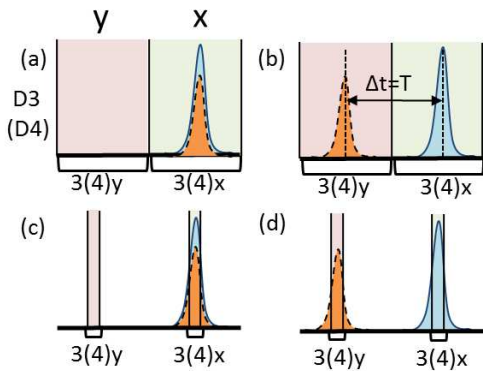


FIG. 2. (Color online) The configurations for the coincidence time windows. Each time window is divided into the two temporal modes x and y . The solid and dashed pulses correspond to the light pulses coming from mode 1 and mode 2, respectively. (a,b) Each of the time windows are set to be much larger than the pulse duration. Two incoming pulses at D3 (D4) are shown with time delay T (a) and without time delay (b). (c,d) Each of the time windows are set to be shorter than the pulse duration for suppressing stray photon detection. Two incoming pulses at D3 (D4) are shown with time delay T (c) and without time delay (d).

II. METHOD

We first review the standard method of time-resolved coincidence detection for the HOM interference experiments. Then we discuss an extended method that reduces an effect of stray photons or accidental coincidences by shortening a coincidence time window even below the coherence time of signal photons.

Let us explain the standard method to observe the HOM interference of two independent light pulses. As shown in Fig. 1, the light pulses in modes 1 and 2 are mixed by a half beamsplitter (HBS) followed by photon detectors D3 and D4. We assume that a relative delay (timing difference) Δt between two incoming light pulses is precisely determined in advance. The delay line is introduced in mode 2 for the adjustment of Δt .

As is well known, by counting the two-fold coincidence events between D3 and D4 with detection time windows much larger than the pulse duration for various values of Δt , the HOM dip will be observed, while the single counts of D3 and D4 take constant values [6–12]. The visibility of the HOM interference is represented by $V = 1 - P_0/P_\infty$, where P_0 and P_∞ are the two-fold coincidence probabilities with $\Delta t = 0$ and $\Delta t = T$, respectively, where T is chosen to be much larger than the pulse duration of input light.

The two-fold coincidence probability P can be understood as follows: As shown in Fig. 2, we assume that a common fixed time window of width $2T$ is adopted for D3 and D4, regardless of the amount of delay Δt . Let us divide the window in two and denote the two halves

by x and y . Figs. 2 (a) and (b) show the sketches of the light pulses with $\Delta t = 0$ and that with $\Delta t = T$, respectively. The light from mode 1 is always detected at the center of x , while the one from mode 2 is detected in x for $\Delta t = 0$ and in y for $\Delta t = T$. Let us denote by $3x$ a detection event at D3 in period x , which may be caused by the input pulse, stray background photons, or dark counting, and define $4x$, $3y$, $4y$ similarly. Then, the coincidence probability P determined in this conventional setup corresponds to the rate of occurrence of event ($3x$ or $3y$) and ($4x$ or $4y$). An underlying assumption in this method is that the contribution of backgrounds should be the same for Figs. 2 (a) and 2 (b), which is satisfied if the statistical properties of stray photons are time-invariant.

If background photons are not negligible, shortening the widths of time windows x and y is favorable. In this case, each width of the time window may be close to or even much shorter than the signal pulse width [14–16], as shown in Fig. 2 (c) and (d). In this paper, we adopt this regime for suppressing stray photons. The coincidence probability P is calculated from the rate of occurrence of event ($3x$ or $3y$) and ($4x$ or $4y$), just as in the conventional setup. The contribution of stray photons should be the same for Figs. 2 (c) and 2 (d) if the statistical properties of stray photons are time-invariant, which is also normally assumed in the conventional setup.

III. EXPERIMENT

A. Photon pair source

Our experimental setup is shown in Fig. 3 (a). An initial beam from an external cavity diode laser (ECDL) working at 1560 nm with a linewidth of 1.8 kHz is frequency doubled by using a periodically-poled lithium niobate waveguide (PPLN/W) [26]. The frequency of the ECDL is stabilized by the saturated absorption spectroscopy of rubidium atoms. The obtained cw light at 780 nm is set to be vertically (V) polarized and is coupled to a 40-mm-long and type-0 quasi-phase-matched PPLN/W. It generates non-degenerate photon pairs at 1541 nm and 1580 nm by SPDC. The V-polarized photons at 1541 nm and 1580 nm are separated into different spatial modes by a dichroic mirror (DM). The photons at 1541 nm are flipped to horizontal (H) polarization by a half-wave plate (HWP), and they are coupled to a polarization maintaining fiber (PMF) followed by a fiber-based Bragg grating (FBG). The photons at 1580 nm are also coupled to a PMF followed by a FBG.

We first characterized our photon pair source by measuring the single counts and the coincidence counts just after the FBGs in Fig. 3 (b). In order to evaluate the photon pair generation efficiency, we set the bandwidths of FBG₁₅₄₁ and FBG₁₅₈₀ to be 1 nm. For preventing the saturation of the detectors, we set the pump power to be $p = 105 \mu\text{W}$. The observed coincidence count rate is $C = 1.8 \times 10^5$ counts/(s·nm) and single count rates are

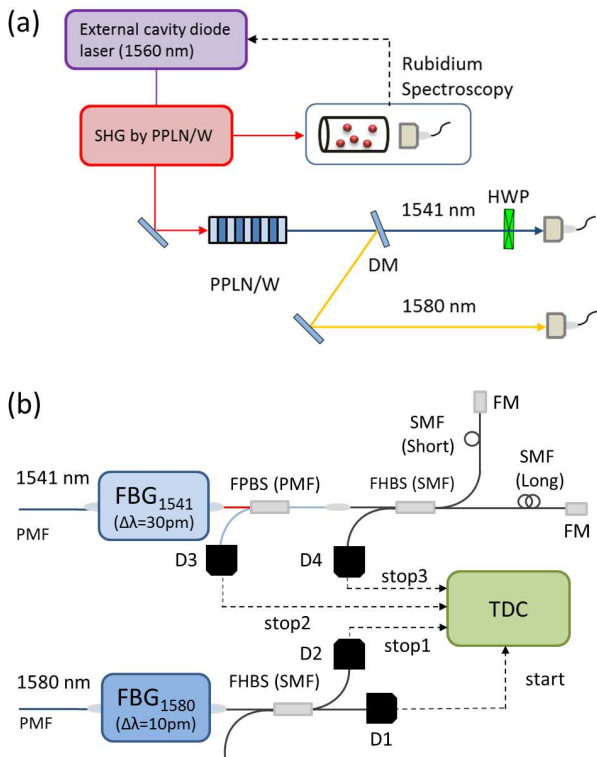


FIG. 3. (Color online) (a) The experimental setup of a photon pair source. The cw pump beam at 780 nm is obtained by the second-harmonic generation based on a periodically-poled lithium niobate waveguide (PPLN/W) pumped by an external cavity diode laser working at 1560 nm. Non-degenerate photon pairs are generated by SPDC by another PPLN/W. (b) The experimental setup of the HOM interference. We performed the experiment of the HOM interference between photons at 1541 nm which are heralded by the photon detection at D1 and D4 with a time difference of Δt .

$S_{1541} = 2.0 \times 10^6$ counts/(s·nm) for 1541 nm and $S_{1580} = 3.0 \times 10^6$ counts/(s·nm) for 1580 nm. The single count rates and the coincidence count rate are represented by $S_{1541} = \gamma p \eta_{1541}$, $S_{1580} = \gamma p \eta_{1580}$ and $C = \gamma p \eta_{1541} \eta_{1580}$, where γ is a photon pair generation efficiency and η_λ is a overall transmittance of the system for the photon at λ nm. We estimated $\gamma = S_{1541} S_{1580} / (C p)$ just after the PPLN/W to be about 3.2×10^8 pairs/(s·mW·nm). When we performed the HOM experiment described in detail later, we connected the output of the FBGs to the fiber-based optical circuit and set the bandwidths of FBG₁₅₄₁ to be 30 pm and FBG₁₅₈₀ to be 10 pm, respectively. In addition, we set the detection window to be 80 ps and the pump power to be 2.5 mW. In this setup, the observed coincidence count rate between detectors D1 and D3 was 1.0×10^3 counts/s.

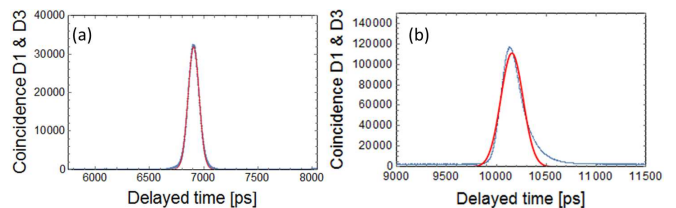


FIG. 4. (Color online) The relations between two-fold coincidence counts and detection timings. The red solid curves are the Gaussian fit to the obtained data. (a) The result of the measurement of the timing jitter. The pump power coupled to PPLN/W is set to be $3.5 \mu\text{W}$, and we directly connected the output of the FBGs (3 nm) to D1 & D2. The other combinations of detectors (D1, D3), (D1, D4) and (D2, D3) are almost the same as (a). (b) The measurement result of the coherence time τ . The pump power coupled to PPLN/W is set to be 2.5 mW, and we used FBG₁₅₈₀ (10 pm) and FBG₁₅₄₁ (30 pm).

B. Detection system

Next, we measured the timing jitter of the overall timing measurement system with superconducting nanowire single-photon detectors (SNSPDs) [27]. For the measurement of the timing jitter, we used bandwidths (3 nm) for FBG₁₅₄₁ and FBG₁₅₈₀ which correspond to the temporal width of 1.2 ps, and measured the arrival time of the picosecond photons by directly connecting the output of the FBGs to the detectors. In this setup, since the temporal width of the photons is sufficiently shorter than the timing jitter of the system, the distribution of arrival time difference of the photons reflects the timing jitter of the system. The typical experimental result is shown in Fig. 4 (a). By fitting the experimental data by Gaussian, the deconvolved timing jitter is estimated to be 85 ps FWHM for all of the four detectors. We also estimated the coherence time τ , which is defined by the temporal width of the photon after FBG₁₅₄₁ (30 pm) heralded by the half of the photon pairs which is filtered by FBG₁₅₈₀ (10 pm). In our experiment, the temporal distribution obtained by the coincidence detection reflects the convolution of τ and timing jitters of the photon detectors. Fig. 4 (b) shows the two-fold coincidence count between D1 and D3, and the fitted Gaussian curve. By subtracting the effect of the timing jitter of each detector from the FWHM of the fitted Gaussian, τ is estimated to be 231 ps FWHM.

C. HOM interference

The HOM interference is performed by using a fiber-based optical circuit as shown in Fig. 3 (b). The photons at 1580 nm are filtered by FBG₁₅₈₀ with a bandwidth of 10 pm. After the FBG, the photons are split into two different spatial modes by a fiber-based half beam-splitter (FHBS) followed by SNSPDs. The photon de-

tections by D1 and D2 with a time difference of Δt heralds two photons at 1541 nm with the same time difference Δt . They are filtered by FBG_{1541} with a bandwidth of 30 pm as shown in Fig. 3 (b). After passing through a fiber-based polarizing beamsplitter (FPBS), the two H-polarized photons propagate in a single-mode fiber (SMF), and they are separated into a long path and a short path by a FHBS. The photons are reflected by a Faraday mirror (FM) at the end of each path, at which the polarizations of the photons are flipped. After going back to the FHBS, the two photons are split into two paths and they are detected by D3 and D4. We note that each of the two photons receives polarization fluctuation in the SMF. In the optical circuit, such fluctuations are much slower than the round-trip time of the photon propagation in each path and thus the birefringence effect in the SMF is automatically compensated after passing through each path by using the FM [28].

We collect the four-fold coincidence events by using a time-digital converter (TDC). The electric signal from D1 is used as a start signal, and the electric signals from D2, D3 and D4 are used as stop signals. When the photons are detected at D1, the histograms of the delayed coincidence counts in the stop signals at D2 and D3 are obtained as shown in Figs. 5 (a) and (b), respectively. In Fig. 5 (b), left peak L and right peak R indicate the events where the photons at 1541 nm passed through the short and long paths, respectively. When we post-select the events where the stop signal of D2 has a delay Δt , additional two peaks L' and R' appear in the histogram of D3 as in Fig. 5 (c), which shows the three-fold coincidence among D1, D2 and D3. The two-fold coincidence between D1 and D4, and the three-fold coincidence among D1, D2 and D4 show almost the same histograms as Fig. 5 (b) and (c), respectively. We chose a value of $\Delta t = t_1$ such that the two peaks L' and R are separated, and defined the timing of the peak L' as y and that of peak R as x . Then we determined the four-fold coincidence count C_∞ from the events where the stop signals of D2, D3 and D4 were recorded at the timings t_1 , (x or y) and (x or y), respectively, with all of the coincidence windows having a width of 80 ps. This corresponds to the situation shown in Fig. 2 (d). If we chose the delay for D2 to be $\Delta t = t_0$ such that peak L' is overlapped on R, the post-selected histogram of the three-fold coincidence among D1, D2 and D3 becomes as shown in Fig. 5 (d). In this case, we determined the four-fold coincidence count C_0 by selecting the stop signals with the timing of t_0 for D2, and (x or y) for D3 and D4. This corresponds to the situation shown in Fig. 2 (c). The visibility is obtained by $V = 1 - C_0/C_\infty$.

We set the pump power coupled to PPLN/W to be 2.5 mW. The total measurement time is 156 hours. By the experimental data, we obtained C_∞ and C_0 as 87 counts and 11 counts, respectively. The observed visibility was 0.87 ± 0.04 . This value is much higher than 0.77 obtained in Ref. [14].

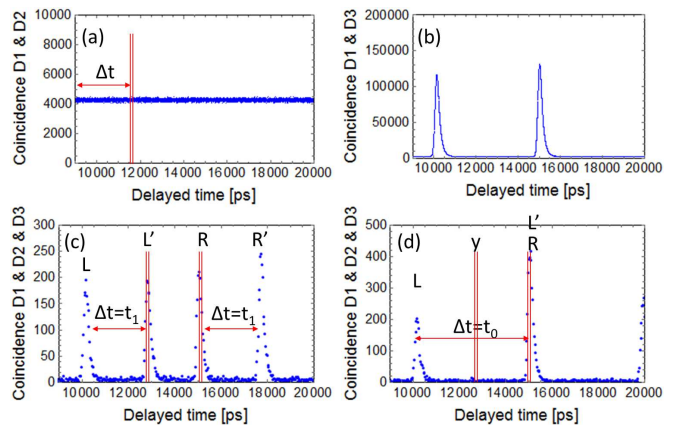


FIG. 5. (Color online) The coincidence counts between (a) D1 & D2 and (b) D1 & D3, respectively. (c) The three-fold coincidence among D1, D2 and D3 for the start signal of D1. The delay time of the stop signal of D2 is chosen to be $\Delta t = 2.6$ ns. (d) The three-fold coincidence among D1, D2 and D3 for the start signal of D1. The delay time is chosen such that Δt is equal to the time lag between photons coming from long and short paths. During the experiment, the pump power coupled to PPLN/W is set to be 2.5 mW.

IV. DISCUSSION

We consider the reason for the degradation of the observed visibility of the HOM interference. In our experiment, since the effect of the timing jitters of the detectors is estimated to be small due to the large coherence time, we only consider the effect of stray photons including multiple pair emission. Below we derive a simple relationship among the visibility and the intensity autocorrelation functions of the signal light pulses and stray photons. For simplicity, we assume that the signal photons and stray photons observed in a time window x or y are in a single mode. We define creation operators of the input and the output light of the HBS as \hat{a}_{ik}^\dagger and \hat{b}_{jk}^\dagger , respectively, where $i = 1, 2$, $j = 3, 4$ and $k = x, y$. The above operators satisfy the commutation relations $[\hat{a}_{ik}, \hat{a}_{i'k'}^\dagger] = \delta_{ii'}\delta_{kk'}$ and $[\hat{b}_{jk}, \hat{b}_{j'k'}^\dagger] = \delta_{jj'}\delta_{kk'}$. As in our experiment, we assume that the transmittance η_i of the system including the detection efficiency of D_i for $i = 3, 4$ is much less than 1 such that the events where two or more photons are simultaneously detected at the single detector are negligible, and the detection probabilities are proportional to the photon number in the detected mode. The two-fold coincidence probability P is expressed as $P = \eta_3\eta_4 \langle (\hat{n}_{3x} + \hat{n}_{3y})(\hat{n}_{4x} + \hat{n}_{4y}) \rangle$, where $\hat{n}_{jk} = \hat{b}_{jk}^\dagger \hat{b}_{jk}$ is the number operator for output modes $j = 3, 4$ and $k = x, y$. P_0 and P_∞ are calculated by using P for the input signal light pulses coming from $1x$ & $2x$ and $1x$ & $2y$, respectively. As is often the case with practical settings, we assume that the signal light pulses and stray photons have no phase correlation and are statistically independent. We characterize the

property of stray photons alone by the average photon number n and the normalized intensity correlation function $g_n^{(2)}$. That is to say, if mode ik does not include the signal light, $\langle \hat{a}_{ik}^\dagger \hat{a}_{ik} \rangle = n$ and $\langle : (\hat{a}_{ik}^\dagger \hat{a}_{ik})^2 : \rangle / n^2 = g_n^{(2)}$ holds. Similarly, we define s and $g_s^{(2)}$ such that, when mode ik includes the signal light as well as stray photons, $\langle \hat{a}_{ik}^\dagger \hat{a}_{ik} \rangle = s$ and $\langle : (\hat{a}_{ik}^\dagger \hat{a}_{ik})^2 : \rangle / s^2 = g_s^{(2)}$ holds. From the definitions, we obtain $P_0 = \eta_3 \eta_4 (s^2 g_s^{(2)} + n^2 g_n^{(2)} + 4sn)/2$ and $P_\infty = \eta_3 \eta_4 (s^2 g_s^{(2)} + n^2 g_n^{(2)} + (s+n)^2)/2$. Here we used a unitary operator \hat{U} of the HBS satisfying $\hat{U} \hat{b}_{3k}^\dagger \hat{U}^\dagger = (\hat{a}_{1k}^\dagger + \hat{a}_{2k}^\dagger)/\sqrt{2}$ and $\hat{U} \hat{b}_{4k}^\dagger \hat{U}^\dagger = (\hat{a}_{1k}^\dagger - \hat{a}_{2k}^\dagger)/\sqrt{2}$. Thus V is represented by

$$V = \frac{(1 - \chi)^2}{g_s^{(2)} + \chi^2 g_n^{(2)} + (1 + \chi)^2}, \quad (1)$$

where $\chi = n/s$. When $n \ll s$, the visibility is approximated by $V = 1/(1 + g_s^{(2)})$, and it takes maximum of $V = 1$ for the input of genuine single photons [29].

In our experimental setup in Fig. 3, the intensity correlation $g_s^{(2)}$ of the signal light could be measured by using the coincidence between D3 and D4 under the heralding of D1, if we run an additional experiment with the short arm detached from the FHBS. Instead, we calculated the same quantity from the same experimental data gathered for the main result. This implies that the determined value $g_{ex}^{(2)}$ includes the contribution of the stray photons coming into FHBS from the short arm. The single count probability $S_{3(4)}$ at D3(4) and coincidence count probability C_{34} between D3 & D4 conditioned on the photon detection at D1 are represented by $S_i = \eta_i(s+n)/2$ and $C_{34} = \eta_3 \eta_4 (s^2 g_s^{(2)} + n^2 g_n^{(2)})/4$. The measured quantity is then given by $g_{ex}^{(2)} \equiv C_{34}/(S_3 S_4) = (g_s^{(2)} + \chi^2 g_n^{(2)})/(1 + \chi)^2$, which is equal to $g_s^{(2)}$ for $\chi = 0$. Using this measured quantity, the visibility in Eq. (1) is represented by

$$V = \frac{(1 - \chi)^2}{(1 + \chi)^2 (1 + g_{ex}^{(2)})}. \quad (2)$$

So far, we have assumed that each detector receives only a single mode per window for simplicity. Rather surprisingly, the relation (S4) still holds when detectors also receives stray photons in other modes, as long as the statistical independence among different modes is fulfilled (see Supplemental Material). From the experimental results of $g_{ex}^{(2)} = 5.3 \times 10^{-2}$ and $\chi = 2.8 \times 10^{-2}$, we obtain $V = 0.85$, which is in good agreement with the observed visibility of 0.87 ± 0.04 within a margin of error. These results indicate that the degradation of the visibility is mainly caused by stray photons. Since the main cause of the stray photons is the accidental emission of photon pairs from SPDC, a higher visibility will be obtained by using a lower pump power and shorter timing selection for the photon detection.

V. CONCLUSION

In conclusion, we have performed an experiment of the HOM interference between two photons produced by the two independent SPDC processes with cw pump light. The observed visibility is 0.87 ± 0.04 , which is much higher than 0.77 observed in Ref. [14]. We also presented a simple relation between the visibility and the second order intensity correlation function, and showed that it holds with a good approximation in this experiment. The relation is convenient for the estimation of the possible visibility from the second order intensity correlation functions of the various input light sources. The results presented here will be useful for many applications such as QKD and quantum repeaters without the necessity of performing active synchronizations of the photon sources.

ACKNOWLEDGMENTS

This work was supported by JSPS Grant-in-Aid for Scientific Research (A) JP16H02214, (B) JP25286077, (B) JP26286068 and (B) JP15H03704. RL, TY and NI were supported by JSPS Bilateral Open Partnership Joint Research Projects. YT was supported by JSPS Grant-in-Aid for JSPS Research Fellow JP16J05093.

-
- [1] C. K. Hong, Z. Y. Ou, and L. Mandel, Phys. Rev. Lett. **59**, 2044 (1987).
[2] J.-W. Pan *et al.*, Rev. Mod. Phys. **84**, 777 (2012).
[3] X.-S. Ma *et al.*, Nature **489**, 269 (2012).
[4] J. Carolan *et al.*, **349**, 711 (2015).
[5] M. Tillmann *et al.*, Nature Photonics **7**, 540 (2013).
[6] H. de Riedmatten, I. Marcikic, W. Tittel, H. Zbinden, and N. Gisin, Phys. Rev. A **67**, 022301 (2003).
[7] T. Yang, Q. Zhang, T. Y. Chen, S. Lu, J. Yin, J. W. Pan, Z. Y. Wei, J. R. Tian, and J. Zhang, Phys. Rev. Lett. **96**, 110501 (2006).
[8] R. Kaltenbaek, R. Prevedel, M. Aspelmeyer, and A. Zeilinger, Phys. Rev. A **79**, 040302 (2009).
[9] P. Aboussouan, O. Alibert, D. B. Ostrowsky, P. Baldi, and S. Tanzilli, Phys. Rev. A **81**, 021801 (2010).
[10] M. Tanida, R. Okamoto, and S. Takeuchi, Opt. Express **20**, 15275 (2012).
[11] A. McMillan *et al.*, Scientific reports **3**, 2032 (2013).
[12] Y. Tsujimoto *et al.*, Opt. Express **23**, 13545 (2015).
[13] M. Zukowski, A. Zeilinger, M. A. Horne, and A. K. Ekert, Phys. Rev. Lett. **71**, 4287 (1993).
[14] M. Halder *et al.*, Nature Physics **3**, 692 (2007).
[15] M. Halder *et al.*, New Journal of Physics **10**, 023027 (2008).
[16] J. Yang, X. H. Bao, H. Zhang, S. Chen, C. Z. Peng, Z. B. Chen, J. W. Pan, Phys. Rev. A **80**, 042321 (2009).

- [17] F. Kaiser *et al.*, Selected Topics in Quantum Electronics, IEEE Journal of **21**, 69 (2015).
- [18] Z.-S. Yuan *et al.*, Nature **454**, 1098 (2008).
- [19] N. Sangouard, C. Simon, H. de Riedmatten, and N. Gisin, Rev. Mod. Phys. **83**, 33 (2011).
- [20] B. C. Jacobs, T. B. Pittman, and J. D. Franson, Phys. Rev. A **66**, 052307 (2002).
- [21] D. Collins, N. Gisin, and H. De Riedmatten, Journal of Modern Optics **52**, 735 (2005).
- [22] H.-K. Lo, M. Curty, and B. Qi, Phys. Rev. Lett. **108**, 130503 (2012).
- [23] S. Pirandola *et al.*, Nature Photonics (2015).
- [24] A. Scherer, B. C. Sanders, and W. Tittel, Opt. Express **19**, 3004 (2011).
- [25] C. Monroe, R. Raussendorf, A. Ruthven, K. R. Brown, P. Maunz, L. M. Duan, J. Kim, Phys. Rev. A **89**, 022317 (2014).
- [26] T. Nishikawa *et al.*, Opt. Express **17**, 17792 (2009).
- [27] S. Miki, T. Yamashita, H. Terai, and Z. Wang, Opt. Express **21**, 10208 (2013).
- [28] A. Muller *et al.*, Applied Physics Letters **70**, 793 (1997).
- [29] R. Ikuta *et al.*, arXiv preprint arXiv:1607.01465 (2016).

SUPPLEMENTAL MATERIAL

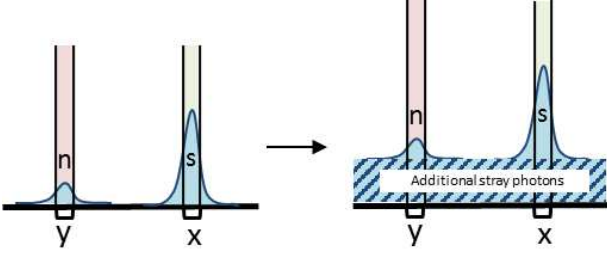


FIG. S1. (Color online) The left figure shows the photon distribution considered in the main text. The right figure presents the sketch in the case where additional stray photons in other modes are detected.

We show that the relation among V , χ and $g_{ex}^{(2)}$ in the main text holds true even under the presence of stationary photon noise in modes different from the signal modes, as long as noise photons in different modes are statistically independent. The situation is shown in Fig. S1. The additional noises accompanying the input signal pulse of mode $1x$ are decomposed into mutually orthogonal modes labeled by index l , and its creation operator is denoted by $\hat{a}_{l,1x}^\dagger$. The signal mode is orthogonal to every noise mode, namely, $[\hat{a}_{1x}^\dagger, \hat{a}_{l,1x}^\dagger] = 0$. We further define the creation operators $\hat{a}_{l,2x}^\dagger$, $\hat{b}_{l,3x}^\dagger$, and $\hat{b}_{l,4x}^\dagger$ such that the four modes with a common index l form the input and output modes of HBS. We define the modes in window y similarly as $\hat{a}_{l,iy}^\dagger$, $\hat{b}_{l,jy}^\dagger$. Let us define sums of the photon number operators by $\hat{N}_{ik} = \sum_l \hat{a}_{l,ik}^\dagger \hat{a}_{l,ik}$ and $\hat{N}_{jk} = \sum_l \hat{b}_{l,jk}^\dagger \hat{b}_{l,jk}$. Since the

noise photons are assumed to be stationary, we have $\langle \hat{N}_{ix} \rangle = \langle \hat{N}_{iy} \rangle$ and $\langle : \hat{N}_{3x} \hat{N}_{4x} : \rangle = \langle : \hat{N}_{3y} \hat{N}_{4y} : \rangle$. Define $N := (\langle \hat{N}_{1x} \rangle + \langle \hat{N}_{2x} \rangle)/2 = (\langle \hat{N}_{1y} \rangle + \langle \hat{N}_{2y} \rangle)/2$.

We first calculate the two-fold coincidence probability $P = \eta_3 \eta_4 \langle : (\hat{n}'_{3x} + \hat{n}'_{3y})(\hat{n}'_{4x} + \hat{n}'_{4y}) : \rangle$ between D3 and D4 in Fig. 1 in the main text, where $\hat{n}'_{jk} = \hat{n}_{jk} + \hat{N}_{jk}$. When the input signal light pulses come from $1x$ & $2x$, one of the four terms in P is calculated as $\langle : \hat{n}'_{3x} \hat{n}'_{4x} : \rangle = \langle : (\hat{n}_{3x} + \hat{N}_{3x})(\hat{n}_{4x} + \hat{N}_{4x}) : \rangle = (\langle : \hat{n}_{1x}^2 : \rangle + \langle : \hat{n}_{2x}^2 : \rangle) + 2\langle \hat{n}_{1x} + \hat{n}_{2x} \rangle \langle \hat{N}_{1x} + \hat{N}_{2x} \rangle / 4 + \langle : \hat{N}_{3x} \hat{N}_{4x} : \rangle = s^2 g_s^{(2)}/2 + 2sN + \langle : \hat{N}_{3x} \hat{N}_{4x} : \rangle$, where $\langle \hat{n}_{1x} \rangle = \langle \hat{n}_{2x} \rangle = s$ and $\langle : \hat{n}_{1x}^2 : \rangle = \langle : \hat{n}_{2x}^2 : \rangle = s^2 g_s^{(2)}$. Here we used $\langle \hat{n}_{ik} \hat{N}_{ik} \rangle = \langle \hat{n}_{ik} \rangle \langle \hat{N}_{ik} \rangle$ from the assumption, and a unitary transformation by the HBS as $\hat{U} \hat{b}_{l,3k}^\dagger \hat{U}^\dagger = (\hat{a}_{l,1k}^\dagger + \hat{a}_{l,2k}^\dagger)/\sqrt{2}$ and $\hat{U} \hat{b}_{l,4k}^\dagger \hat{U}^\dagger = (\hat{a}_{l,1k}^\dagger - \hat{a}_{l,2k}^\dagger)/\sqrt{2}$ in addition to the transformation of the signal modes. Similarly, $\langle : \hat{n}'_{3y} \hat{n}'_{4y} : \rangle$ is calculated as $n^2 g_n^{(2)}/2 + 2nN + \langle : \hat{N}_{3x} \hat{N}_{4x} : \rangle$, where $\langle \hat{n}_{1y} \rangle = \langle \hat{n}_{2y} \rangle = n$ and $\langle : \hat{n}_{1y}^2 : \rangle = \langle : \hat{n}_{2y}^2 : \rangle = n^2 g_n^{(2)}$. $\langle \hat{n}'_{3x} \hat{n}'_{4y} \rangle$ and $\langle \hat{n}'_{4x} \hat{n}'_{3y} \rangle$ are calculated as $sn + N(s+n) + N^2$. As a result,

$$P_0 = \eta_3 \eta_4 ((s^2 g_s^{(2)} + n^2 g_n^{(2)})/2 + 2N^2 + 4N(s+n) + 2sn + 2\langle : \hat{N}_{3x} \hat{N}_{4x} : \rangle). \quad (S1)$$

On the other hand, when the input signal light pulses come from $1x$ & $2y$, $\langle : \hat{n}'_{3x} \hat{n}'_{4x} : \rangle$ and $\langle : \hat{n}'_{3y} \hat{n}'_{4y} : \rangle$ are calculated as $(s^2 g_s^{(2)} + n^2 g_n^{(2)})/4 + N(s+n) + \langle : \hat{N}_{3x} \hat{N}_{4x} : \rangle$. Similarly, $\langle \hat{n}'_{3x} \hat{n}'_{4y} \rangle$ and $\langle \hat{n}'_{3y} \hat{n}'_{4x} \rangle$ are calculated as $(s+n)^2/4 + N(s+n) + N^2$. As a result, we obtain

$$P_\infty = \eta_3 \eta_4 ((s^2 g_s^{(2)} + n^2 g_n^{(2)})/2 + 2N^2 + 4N(s+n) + (s+n)^2/2 + 2\langle : \hat{N}_{3x} \hat{N}_{4x} : \rangle). \quad (S2)$$

Next, we introduce the relation among $g_{ex}^{(2)}$, $g_s^{(2)}$ and $g_n^{(2)}$ in our experimental setup in Fig. 3 in the main text. The single count $S_{3(4)}$ at D3(4) and coincidence count C_{34} between D3 & D4 conditioned on the photon detection at D1 are described by $S_{3(4)} = \eta_{3(4)}(s+n+2N)/2$, and $C_{34} = \eta_3 \eta_4 (s^2 g_s^{(2)} + n^2 g_n^{(2)} + 4N(s+n) + 4\langle : \hat{N}_{3x} \hat{N}_{4x} : \rangle)/4$. The observed correlation function is expressed as

$$g_{ex}^{(2)} = \frac{C_{34}}{S_3 S_4} = \frac{s^2 g_s^{(2)} + n^2 g_n^{(2)} + 4N(s+n) + 4\langle : \hat{N}_{3x} \hat{N}_{4x} : \rangle}{(s+n+2N)^2} \quad (S3)$$

By combining equation (S1), (S2) and (S3), the visibility $V = 1 - P_0/P_\infty$ is described by

$$V = \frac{(1-\chi)^2}{(1+\chi)^2(1+g_{ex}^{(2)})}, \quad (S4)$$

where $\chi = (n+N)/(s+N)$.